The Astrophysical Journal, 977:177 (10pp), 2024 December 20 https://doi.org/10.3847/1538-4357/ad84de

Varying Activity and the Burst Properties of FRB 20240114A Probed with GMRT Down to 300 MHz

Ajay Kumar, Yogesh Maan, and Yash Bhusare
National Centre for Radio Astrophysics (NCRA–TIFR), Pune–411007, India; akumar@ncra.tifr.res.in, ymaan@ncra.tifr.res.in, ybhusare@ncra.tifr.res.in
Received 2024 June 3; revised 2024 October 1; accepted 2024 October 1; published 2024 December 11

Abstract

Repeating fast radio bursts (FRBs) can exhibit a wide range of burst repetition rates, from none to hundreds of bursts per hour. Here we report the detection and characteristics of 60 bursts from the recently discovered FRB 20240114A, observed with the upgraded Giant Metrewave Radio Telescope in the frequency ranges 300–500 MHz and 550–750 MHz. The majority of the bursts show narrow emission bandwidth with $\Delta\nu/\nu \sim 10\%$. All of the bursts we detect are faint (<10 Jy ms) and thus probe the lower end of the energy distribution. We determine the rate function for FRB 20240114A at 400 MHz and downward drift rates at 400 and 650 MHz, and we discuss our measurements in the context of the repeating FRB population. We observe sudden variations in the burst activity of FRB 20240114A over time. From our data and the publicly available information on other observations of FRB 20240114A so far, there is an indication that FRB 20240114A potentially exhibits chromaticity in its burst activity. While the burst properties of FRB 20240114A are similar to other repeating FRBs, the frequency-dependent activity, if established, could provide crucial clues to the origin of repeating FRBs. We also place the most stringent 5σ upper limits of 600 and 89 μJy on any persistent radio source (PRS) associated with FRB 20240114A at 400 and 650 MHz, respectively, and compare these with the luminosity of the known PRSs associated with FRB 121102A and FRB 190520B.

Unified Astronomy Thesaurus concepts: Radio transient sources (2008)

1. Introduction

Fast radio bursts (FRBs) are coherent bright radio flashes of cosmological origin with duration ranging from a few microseconds to several milliseconds. Their exceptionally high dispersion measure (DM) along the line of sight cannot be explained by the Galactic electron content, thus predicting their extragalactic origin. The extragalactic nature is now confirmed with several repeating FRBs localized to a variety of galaxies (S. Chatterjee et al. 2017; K. W. Bannister et al. 2019; S. Bhandari et al. 2020; K. E. Heintz et al. 2020; B. Marcote et al. 2020). The origin and emission mechanism of FRBs still remain open questions. Currently, there are ∼800 published FRBs, of which some are repeating in nature. Discovery of the first repeating FRB, FRB 20121102A (L. G. Spitler et al. 2014), ruled out cataclysmic events as the source for repeating FRBs. Currently there are close to 60 repeaters known,[1] but only a few are known to be extremely active occasionally. A few repeating FRBs show periodicity in their activity, e.g., FRB 180916 exhibits a periodicity of 16.35 days, while FRB 121102A shows a tentative periodicity of 157 days (CHIME/FRB Collaboration et al. 2020a; K. M. Rajwade et al. 2020). Some FRBs also show very high bursts rates (>100 bursts hr^{-1}) occasionally, e.g., FRB 201124A and FRB 220912A (D. J. Zhou et al. 2022; Y. Feng et al. 2023). Several repeaters have been followed up or monitored over a long duration of time and their properties are very well studied, but we still we do not have source models that can explain all their observed properties. Discovery of highly active repeaters can provide more detailed insights into the observed spectrotemporal properties like narrowband emission behavior and downward-drifting pattern that have been seen across all repeaters (J. W. T. Hessels et al. 2019; E. Fonseca et al. 2020; Z. Pleunis et al. 2021a).

Recently, CHIME reported the discovery of a highly active repeating FRB, FRB 20240114A (K. Shin & CHIME/FRB Collaboration 2024). Starting on 2024 January 14, CHIME/FRB detected three bursts from FRB 20240114A within two weeks, and at a DM of 527.7 pc cm^{-3} consistent for all the bursts. The CHIME/FRB daily exposure time of only 4 minutes for this source suggested a high burst rate above the fluence thresholds of ∼1 Jy ms (K. Shin & CHIME/FRB Collaboration 2024). There were prompt follow-up observations from various telescopes, including Parkes, FAST, and ours, using various frequency bands (300–500 MHz, 550–750 MHz, and 1060–1460 MHz) of the upgraded Giant Metrewave Radio Telescope (uGMRT; Y. Gupta et al. 2017), which confirmed the high activity of FRB 20240114A (A. Kumar et al. 2024; D. Pelliciari et al. 2024a; P. A. Uttarkar et al. 2024).

Subsequently, FRB 20240114A was localized to an arcsecond precision by the MeerKAT telescope (J. Tian et al. 2024). Following this localization, we focused on low-frequency study of FRB 20240114A using band 3 (300–500 MHz) of the uGMRT. One of our observations was on March 5, when there was a burst storm as reported by FAST (J. Zhang et al. 2024a). Since then, several other detections have been reported from *P* band to frequencies up to 6 GHz (D. M. Hewitt et al. 2024; P. Joshi et al. 2024; A. Kumar et al. 2024; O. S. Ould-Boukattine et al. 2024a, 2024b; U. Panda et al. 2024a; D. Pelliciari et al. 2024a, 2024b; K. Shin & CHIME/FRB Collaboration 2024; M. P. Snelders et al. 2024;

[1] https://www.chime-frb.ca/repeaters

J. Tian et al. 2024; P. A. Uttarkar et al. 2024; J. Zhang et al. 2024a, 2024b).

Low-frequency studies of active repeating FRBs provide constraints to various proposed progenitor models for repeating FRBs (e.g., I. Pastor-Marazuela et al. 2021). They also help in studying some of the propagation effects and the underlying emission mechanism (Z. Pleunis et al. 2021b; A. Gopinath et al. 2024). Narrowband behavior has been reported for repeating FRBs (P. Kumar et al. 2021), and it has also been linked to giant pulses from pulsars and magnetars (Y. Maan et al. 2019). Magnetars appear to be the plausible originators of some of the repeating FRBs, especially since the detection of a millisecond duration burst from the Galactic magnetar SGR 1935+2154 with an energy comparable to the faintest FRBs (C. D. Bochenek et al. 2020; CHIME/FRB Collaboration et al. 2020b). The low-frequency observations further help in studying the wide-band spectral behavior of FRBs and probe any potential chromatic evolution of the activity (I. Pastor-Marazuela et al. 2021; Z. Pleunis et al. 2021b).

In this paper, we report detection of 60 bursts at low radio frequencies and narrowband emission from FRB 20240114A. We present the results from the observations done in band 4 (550–750 MHz), band 3 (300–500 MHz) and band 5 (1060–1460 MHz) of the uGMRT. We describe the observation and the search procedure in Section 2 and the rate function at 400 MHz and extreme narrowband emission in Section 3. Burst properties are detailed in Section 3, and we discuss the implications of our results for observed properties of the repeating FRBs and their proposed formation channels in Section 5. Finally, we conclude in Section 6.

2. Observations and Search Procedure

Following a possible high level of activity from the repeating FRB 20240114A reported by K. Shin & CHIME/FRB Collaboration (2024), we conducted prompt follow-up observations using the uGMRT. We utilized the wide frequency coverage of the uGMRT, spanning 300–1460 MHz. Specifically, we observed the source for 114 minutes in band 4 (550–750 MHz) on 2023 February 1; 104 and 71 minutes in band 3 (300–500 MHz) on 2023 February 8 and 12, respectively; and 65 minutes in band 5 (1060–1460 MHz) on 2023 February 13. These observations utilized recording in three different beams: phased-array (PA) beam and the PA spectral voltage (PASV; spectral voltage recording at the Nyquist rate) beam utilizing antennas in compact configuration, and the incoherent-array (IA) beam. We simultaneously recorded the interferometric visibility data with a sampling time of 0.67 s to potentially localize the source within a few arcseconds using a burst with adequate signal-to-noise ratio (S/N). On 2024 February 12, we formed four PA beams with different antenna configurations to potentially obtain a localization better than the position known at that time (about 1.″5 uncertainty; K. Shin & CHIME/FRB Collaboration 2024).

Sensitivity of our above observations was limited, as the actual source was about 1.′2 away from the best estimated position at that time. After FRB 20240114A was localized by MeerKAT to R.A. $= 21^{h}27^{m}39\overset{s}{.}83$ and decl. $= 04^{d}19'46\overset{''}{.}02$ (J. Tian et al. 2024) with precision of about an arcsecond, we followed it for 6 hr more at band 3, now utilizing the full sensitivity of the PA beams. Observations were done in three epochs on 2024 March 5, 8, and 24, with the cumulative on-source times of 55, 85, and 75 minutes, respectively. More recently, we also had two observations at band 4, on 2024 May 29 and 2024 June 15, with cumulative on-source times of 126 minutes in each. The summary of all the observations is detailed in Table 1. In each of these sessions, we recorded the PA beam with 4096 frequency channels and a time resolution of 655 μs. PASV data were also recorded simultaneously, which were coherently dedispersed and converted to filter-bank format with 1024 frequency channels and a time resolution of 81.92 μs in the offline processing.

In all the above sessions, we used the following reduction and search procedures. The raw data were recorded with 16,384, 4096, and 4096 frequency channels and with time resolutions of 655.36, 327.28, and 163.84 μs in bands 3, 4, and 5, respectively. For the band 3 observations conducted in March, we converted the PASV data to filter-bank format with a sampling time of 81.92 μs and 1024 frequency channels. All these raw data were passed through a number of radio frequency interference (RFI) excision rounds as follows. First, RFIClean[2] (Y. Maan et al. 2021) is used to mitigate periodic, broadband, and spiky RFI as well as convert the data to SIGPROC filter-bank format. Subsequently, `dedisperse` from *SIGPROC* is used to subband the data to 1024 frequency channels, followed by one more round of RFI mitigation using RFIClean. Finally, we executed `rfifind` from *PRESTO* (S. Ransom 2011) to compute a mask of further identified RFI-contaminated segments in the data.

We used `prepdata` from PRESTO to dedisperse over a range of DMs from 522 to 532 pc cm^{-3}, with a step of 0.1 pc cm^{-3} for band 3 and 0.2 pc cm^{-3} for band 4. The dedispersed time series were then searched for single pulses using `single_pulse_search.py` above S/N of 7 and with a maximum boxcar width of 0.5 s. The candidates were clustered in arrival times and DM, and then the candidate corresponding to the highest S/N in the individual clusters was verified visually using the waterfall plot prepared using the package `your` (K. Aggarwal et al. 2020).

For the subband search, we divided the 200 MHz bandwidth in bands 4 and 3 into seven subbands. Each subband has a bandwidth of 50 MHz, and their central frequency varies from 325 to 475 MHz for band 3 and from 575 to 725 MHz for band 4, in steps of 25 MHz. Thus, there is 50% overlap between successive subbands. The dedispersion for these subbands is realized by ignoring the frequency channels not desired for a particular subband. The remaining part of the search procedure is the same as described earlier.

In the top panel of Figure 1, we show the detection and nondetection of bursts reported at different frequencies in four different ranges, 0.3–0.8 GHz, 0.8–2.2 GHz, 2.2–4 GHz, and 4–6 GHz, over the duration from 2024 January 14 to May 9 roughly every 10 days. Here we use the limited information that is available from various Astronomer's Telegrams (ATELs) published during this period.

3. Burst Analysis and Results

We detected 10 bursts from our band 3 and band 4 observations conducted before the source was well localized (J. Tian et al. 2024). In these observations, the pointing center was offset from the actual source position by 1.′2 (J. Tian et al. 2024). Of the 10 bursts, 5 were detected in band 4 (550–750 MHz) with an on-source time of 114 minutes, but

[2] https://github.com/ymaan4/RFIClean

Table 1
Details of the Observations

Date	Frequency Range	$N_{\rm antenna}$ (IA)[a]	$N_{\rm antenna}$ (PA)[b]	Visibilities Resolution (s)	$T_{\rm obs}$ (min)
2024 Feb 1	550–750 MHz	19	13	0.67	114
2024 Feb 8	300–500 MHz	18	11	0.67	104
2024 Feb 12	300–500 MHz	⋯	13	0.67	71
2024 Feb 13	1060–1460 MHz	19	5	0.67	65
2024 Mar 5	300–500 MHz	⋯	21	10.7	55
2024 Mar 8	300–500 MHz	⋯	21	10.7	85
2024 Mar 24	300–500 MHz	⋯	22	10.7	75
2024 May 29	550–750 MHz	⋯	21	10.7	126
2024 Jun 15	550–750 MHz	⋯	23	10.7	126

Notes. $T_{\rm obs}$ is the total on-source time.
[a] No. of antennae in the IA mode.
[b] No. of antennae in the PA mode.

only in the IA beam, indicating that the actual source position was offset by more than the PA beamwidth (1.′1). Additionally, we detected five bursts in band 3 in the PA beam despite the offset, as the PA beamwidth was adequately larger at these lower frequencies. We corrected the measured fluences for these observations to account for the offset from the actual position. The correction factor is estimated simply as the ratio of the telescope's sensitivity at the pointing center and the actual source position. Consequently, we estimate the burst rate to be 2.6 $\rm hr^{-1}$ at 650 MHz above the fluence of 0.64 Jy ms, 7 days after CHIME detected two bright bursts from FRB 20240114A (K. Shin & CHIME/FRB Collaboration 2024).

From our later observations in 2024 March, conducted in band 3 (300–500 MHz) and now using the improved position estimate, we detected significant activity. On 2024 March 5, approximately 3 hr and 15 minutes after a FAST observation wherein a sudden extremely high activity (burst rate of 500 $\rm hr^{-1}$ above a fluence of 0.015 Jy ms; J. Zhang et al. 2024a) was noticed, we detected about 27 bursts within 52 minutes, implying a burst rate of 31 $\rm hr^{-1}$ at a fluence threshold of 0.2 Jy ms. The rate varies significantly over short durations, as we detected only five bursts on 2024 March 8, and all within the first 10 minutes out of nearly 75 minutes of the total on-source time. The rate seemed to have decreased by a factor of 8 in 3 days. Later on, with observation on May 29 and June 15, we detected three very faint bursts in the later session. We do not provide burst analysis with bursts detected in band 4. In addition, there were several bursts reported at *P* and *L* bands after this session (D. M. Hewitt et al. 2024; P. Joshi et al. 2024; O. S. Ould-Boukattine et al. 2024a; M. P. Snelders et al. 2024), implying varying activity level. On March 24, we detected 15 bursts from an on-source time of 75 minutes. We did not detect any burst from our band 4 session on 2024 May 29.

In total, we detected 52 bursts in band 3 (300–500 MHz) and 8 bursts in band 4 (550–750 MHz). Some of these bursts exhibit a downward-drifting pattern, and majority of them are narrowband in nature, as shown in Figure 1. Many bursts are primarily centered in the higher part of band 3, i.e., above 400 MHz, as evident from Figure 2; however, it is most likely caused by typically more RFI contamination in the central and lower half of band 3.

3.1. Rate Function

For each of the bursts, we use the filter-bank files and the RFI mask described in Section 2, to prepare a time series dedispersed at the detection DM (i.e., the DM that maximizes the S/N). We extract the time series around the burst's arrival time and normalize the time series in units of the rms noise measured from the off-pulse region. The time series is then calibrated to Jy units using the radiometer equation. To obtain the fluence for each burst, we summed the calibrated time series around the pulse region. After measuring the fluence for each pulse, we characterize the rate function of FRB 20240114A at 400 MHz. Figure 3 shows the log N–log S plot. We fitted a power law using the optimization function `scipy.optimize.minimize`, taking into account Poissonian errors as described by W. Cash (1979). All bursts have fluences below 10 Jy ms, suggesting that we are probing the lower end of the energy distribution. However, there have also been bright bursts reported with fluences in excess of 10 Jy ms at *P* band (O. S. Ould-Boukattine et al. 2024a; D. Pelliciari et al. 2024b).

To measure the pulse widths, we used the `scipy` module `curve_fit` to fit a Gaussian profile to each of the bursts (components). The pulse widths range from 0.6 to 17 ms. The median pulse width of FRB 20240114A at 400 MHz is 4.3 ms, which is broader compared to 1.4 ms at 650 MHz (U. Panda et al. 2024b). The median for the S/N-optimized DM is 528.1 pc $\rm cm^{-3}$. However, we do not take into account scatter broadening while fitting a Gaussian function to the time profile of bursts.

3.2. Emission Bandwidths

To characterize the emission bandwidth, we first downsample the data from 1024 to 128 frequency channels and then average along the time axis around the burst region to estimate the average burst spectrum, as illustrated in the right panel of Figure 2. The average spectrum is fitted with a Gaussian function to estimate the peak frequency and the emission bandwidth (FWHM). More than 95% of the bursts exhibit narrowband emission, as also apparent in Figure 1.

In Figure 2, two major trends are apparent. First, the peak emission frequency seems to decrease (roughly from 480 to 440 MHz) as the emission bandwidth increases from about 20 to 60 MHz. This is most likely caused by the band-edge and search-sensitivity effects—near the top band edge, we might be

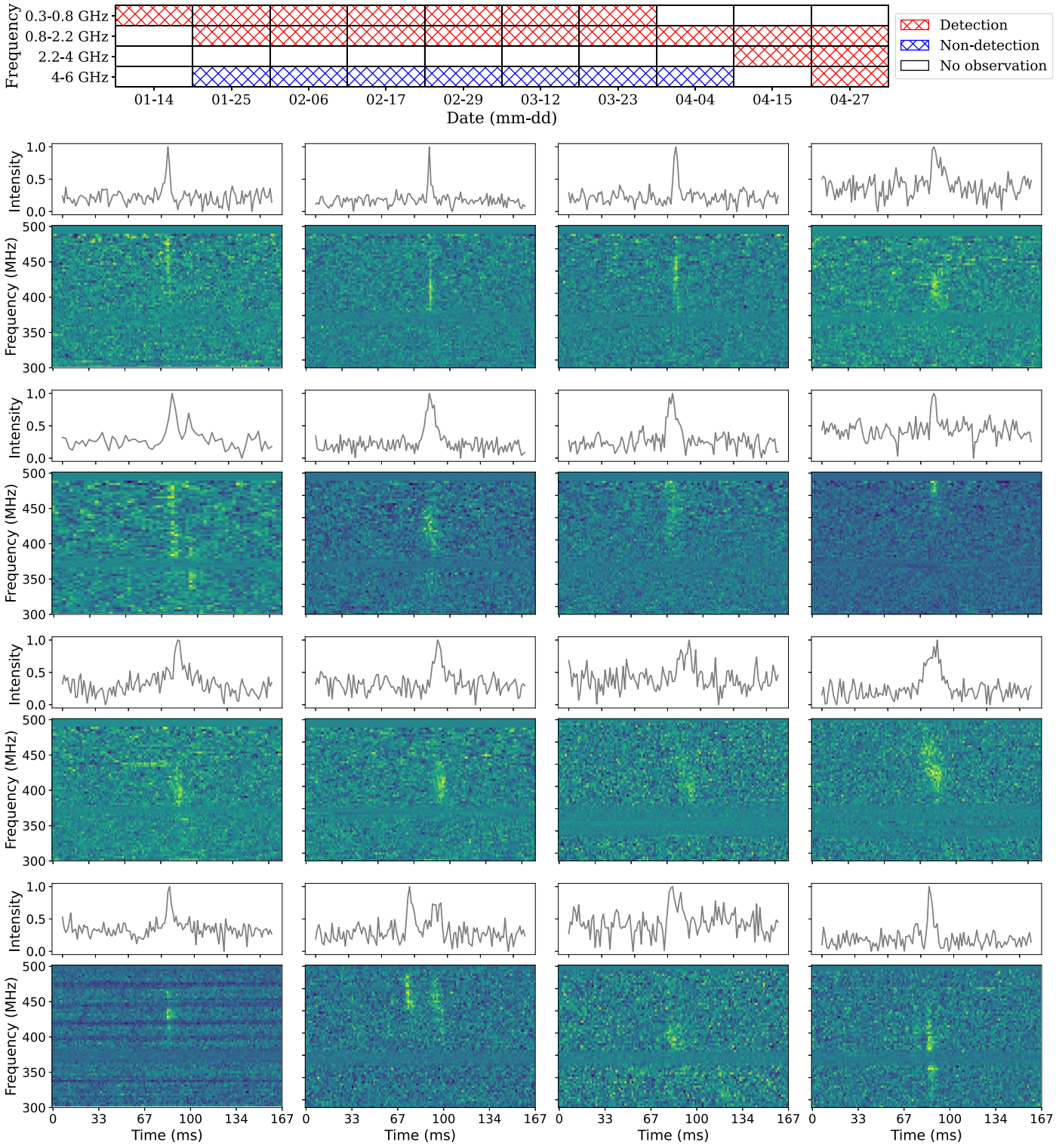

Figure 1. Top: a summary of the observations and detection/nondetection of bursts reported at different frequencies, ranging from *P* band to *C* band, over the duration from 14/01/2024 January 14 to May 9. The data used here are from various ATELs published between 2024 January 28 and May 9 (D. M. Hewitt et al. 2024; P. Joshi et al. 2024; A. Kumar et al. 2024; P. Limaye & L. Spitler 2024; O. S. Ould-Boukattine et al. 2024a, 2024b; U. Panda et al. 2024a; D. Pelliciari et al. 2024a, 2024b; K. Shin & CHIME/FRB Collaboration 2024; M. P. Snelders et al. 2024; J. Tian et al. 2024; P. A. Uttarkar et al. 2024; J. Zhang et al. 2024a, 2024b). Bottom: dynamic spectra and time series of some of the bursts detected at band 3 (300–500 MHz).

seeing only parts of the burst emission otherwise continuing outside our observing bandwidth. A similar but inverted trend would be expected at the lower edge of the band, and we see some hints of it. However, several parts of the spectrum in the lower half of the band (300–400 MHz) are typically contaminated by RFI, which effectively degrades the sensitivity in this part of the band. Consequently, we see this inverted trend effectively starting from roughly around the middle of the

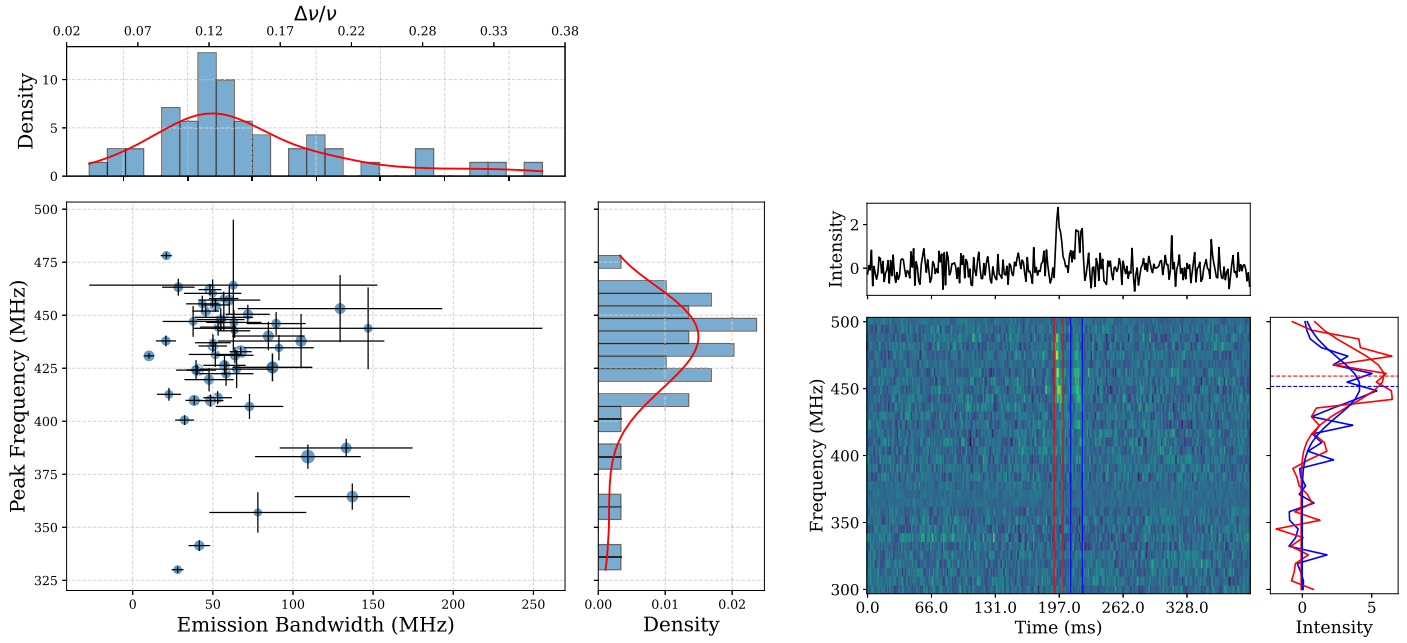

Figure 2. Left: variation of the measured peak frequency with the emission bandwidth. The red line denotes the Gaussian kernel density function for the distribution of the fractional emission bandwidth ($\Delta\nu/\nu$) at top and for the peak frequency at right. Right: example of a burst showing a downward-drifting pattern and Gaussian fits to the spectra for each component. At right, spectra obtained from averaging along the time axis for the regions marked in the left panel under each component are shown. The red and green horizontal lines indicate the peak frequency for each of the components.

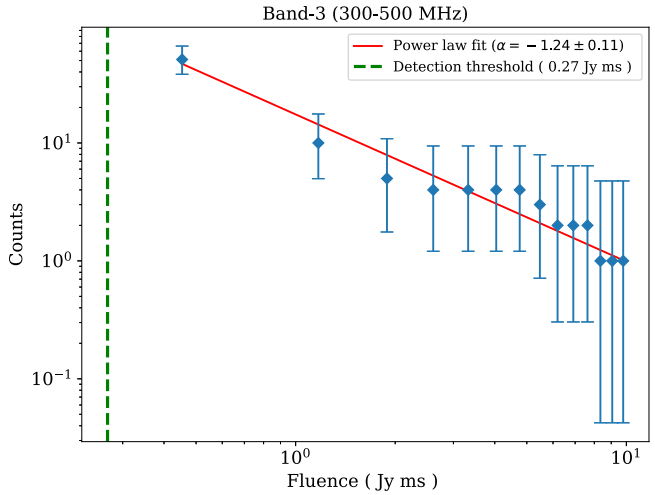

Figure 3. Cumulative distribution of the fluences of the bursts detected at band 3 (300–500 MHz). The green dashed line indicates the fluence threshold for a 2 ms burst detected at an S/N of 10. The red line indicates the fitted power law.

band. The distribution of the peak frequencies peaking around 450 MHz is also a consequence of the above band-edge effects. Figure 2 demonstrates that the emission is narrowband for nearly all the bursts. The fractional bandwidth distribution peaks around 0.12.

3.3. Frequency Drift Rates

The downward-drifting pattern is characteristic of repeating FRBs, with different repeating FRBs showing a wide variety of drift rates ranging from −1 to −60 MHz ms^{-1} (Z. Pleunis et al. 2021a). Many of the bursts exhibit this downward drifting with single and multiple subbursts. The drift rates are typically estimated by first determining the structure-optimized DM and then exploiting two-dimensional correlation. Due to the low S/N of our bursts, we could not utilize `DM_phase`[3] (A. Seymour et al. 2019) for determining the structure-optimized DM. We also could not use `frbgui`[4] (M. A. Chamma et al. 2023) for the same reason. Hence, we use the S/N-optimized DM to measure the relative time of arrivals (TOAs) and the central frequencies of the successive components in multicomponent bursts to estimate the drift rate. The peak frequencies of the subbursts are estimated as described in Section 3.2. The relative TOAs are determined by fitting a Gaussian function to each component in the band-averaged time profile. There are three bursts for which we could measure drift rates. One example of a burst for which we measured the drift rate is shown in the right panel of Figure 4. The drift rate for this burst is estimated to be -0.35 ± 0.07 MHz ms^{-1}. For the other bursts, the drift rates are estimated to be -11.7 ± 0.8 MHz ms^{-1} and -2.07 ± 0.14 MHz ms^{-1}. These measurements are comparable to the drift rates obtained for other repeaters at similar frequencies, as shown in Figure 4.

Using the data made publicly available by U. Panda et al. (2024b), we also measure drift rates for four bursts detected at band 4 that show well-separated, drifting components. The arrival times of the components are provided by the authors, and we estimate the corresponding peak frequencies visually. We liberally assign large uncertainties (3%–6%) to these visual estimates of peak frequencies, which often cover at least half of the total emission bandwidth for the respective components. The drift rates thus estimated are also shown in Figure 4.

4. Imaging Analysis and Results

Our observations in February (at both band 3 and band 4) utilized recording of the interferometric visibilities at 0.67 s

[3] https://github.com/danielemichilli/DM_phase
[4] https://github.com/mef51/frbgui

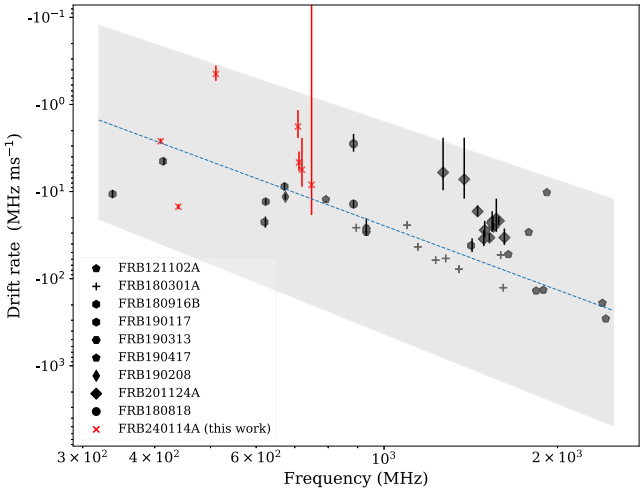

Figure 4. Drift rates as a function of frequency, with both quantities in the rest frame of the respective host galaxy, for FRB 20240114A and other repeaters (e.g., FRB 121102A, FRB 180916B). The dashed blue line and the region shaded around it indicate the power-law fit with its uncertainty, fitted by W.-Y. Wang et al. (2022). References for measurements on other FRBs: J. W. T. Hessels et al. (2019), CHIME/FRB Collaboration et al. (2019), V. R. Marthi et al. (2020), I. Pastor-Marazuela et al. (2021), D. J. Zhou et al. (2022), P. Kumar et al. (2023).

integration time with the aim of localizing the source to arcsecond precision (the position uncertainty at that time was about 1.′5 K. Shin & CHIME/FRB Collaboration 2024). However, these observations did not result in detection of a burst with adequately high S/N for such a localization. Once the source was localized to arcsecond precision by J. Tian et al. (2024), our remaining observations in band 3 used the new position as the pointing center with an integration time of 10.7 s. For band 3 observations, we used 3C 48 as the flux calibrator, and for band 4, we used 3C 147 and 3C 48 in different sessions, and with J2130+050 as the phase calibrator in all the observations. We used `CAPTURE`[5] (R. Kale & C. H. Ishwara-Chandra 2021) for RFI flagging and calibration of the data.

After calibrating the data, we used CASA task `tclean` for imaging, with the deconvolution algorithm set to `MTMFS` and the Briggs weighting scheme (robust = 0). Self-calibration was performed until convergence to an image was achieved. We used `uGMRTprimarybeam` for primary beam correction for the band 4 image obtained from the 2024 February 1 session, since our pointing was slightly offset from the source position. From this observation, we place an upper limit of 140 μJy (at 5σ level) on any continuum emission associated with the FRB (A. Kumar et al. 2024). From our more recent observation on 2024 June 15 we do not detect any continuum emission at the source position, and hence we place the most stringent 5σ upper limit of 89 μJy for continuum emission from any associated persistent radio source (PRS)[6] or the host galaxy at 650 MHz (U. Panda et al. 2024b placed a 5σ upper limit of 124 μJy at the same frequency). Similarly, at band 3 we obtained the final images individually for the data sets from the March 5, 8, and 24 observations. In the best image, we do not detect any continuum emission at the source position up to 600 μJy (at 5σ level), with an on-source time of 78 minutes. We note that there is a bright (325 mJy) source between the FWHM and first null of the uGMRT primary beam. Thus, deconvolution errors limit the rms noise achievable for the band 3 image despite the longer on-source time. We provide the upper limits for spectral luminosity at 650 and 400 MHz using the redshift of 0.13 (M. Bhardwaj et al. 2024). We also obtain an image in band 5 with an on-source time of 65 minutes, but the observations were heavily affected by RFI. Nevertheless, we provide an upper limit of 1 mJy for the PRS at 1.26 GHz using these band 5 data. Figure 5 [7] shows the comparison of our upper limits on emission from a PRS associated with FRB 20240114A, along with that for PRSs associated with FRB 121102A and FRB 190520B, and upper limits on similar emission from various repeating and nonrepeating FRBs, as well as SGR 1935+2154.

5. Discussion

Our efforts to understand the nature of FRB 20240114A included a prompt follow-up in 2024 February and March, at bands 3 and 4 of the uGMRT, right after its discovery. From the observation on February 1 at band 4, we detected bursts in the IA beam but not in the PA beam, suggesting that the position reported by CHIME was offset from the actual source position by at least 1.′1 (i.e., half-power beamwidth), a finding later confirmed by the MeerKAT localization (J. Tian et al. 2024). Subsequent observations in bands 3 and 5 also did not result in bursts adequately bright enough to localize the source. In these early observations, we detected five bursts in band 3 in the PA beam (but not in the IA beam, as these were all faint bursts) and none at band 5. With these detections, we confirmed the high-activity phase of FRB 20240114A in the 300–750 MHz frequency range (A. Kumar et al. 2024). Using the subsequent observations in March, now with adequately precise position estimates from MeerKAT, we measure significant variations in the activity levels of FRB 20240114A, which could be related to the underlying emission mechanism or propagation effects. While two repeating FRBs show periodic modulation in their activity (Chime/FRB Collaboration et al. 2020a; K. M. Rajwade et al. 2020), a few others show high-activity phases (e.g., burst storms) followed by a long quiescence and with no significant periodicity (A. E. Lanman et al. 2022). Currently, there is no clear picture as to what causes such modulations, periodic or otherwise, in the bursting activity.

5.1. Frequency-dependent Activity

FRB 20240114A has been followed up by various telescopes at a variety of observing frequencies covering the range 0.3−6 GHz. We compiled a summary of these observations and burst detections reported by various groups through ATELs and show it in Figure 1. Limited by the details provided in various ATELs, as well as for the convenience of displaying, we quantize the observing frequency into four ranges: 0.3–0.8 GHz, 0.8–2 GHz, 2–4 GHz, and 4–6 GHz. Similarly, the time span between the discovery and the first week of May is divided into 10 parts. We note that at L band and lower frequencies (i.e., the first two frequency ranges) bursts from FRB 20240114A have been detected regularly. However, at the frequencies higher than 2 GHz bursts have been detected only in the later half of April and the beginning

[5] https://github.com/ruta-k/CAPTURE-CASA6

[6] During the review of this paper, X. Zhang & W. Yu (2024) have suggested the presence of an associated continuum emission of 72 ± 14 μJy at 1.3 GHz.

[7] $L\nu$ is calculated assuming a flat spectrum.

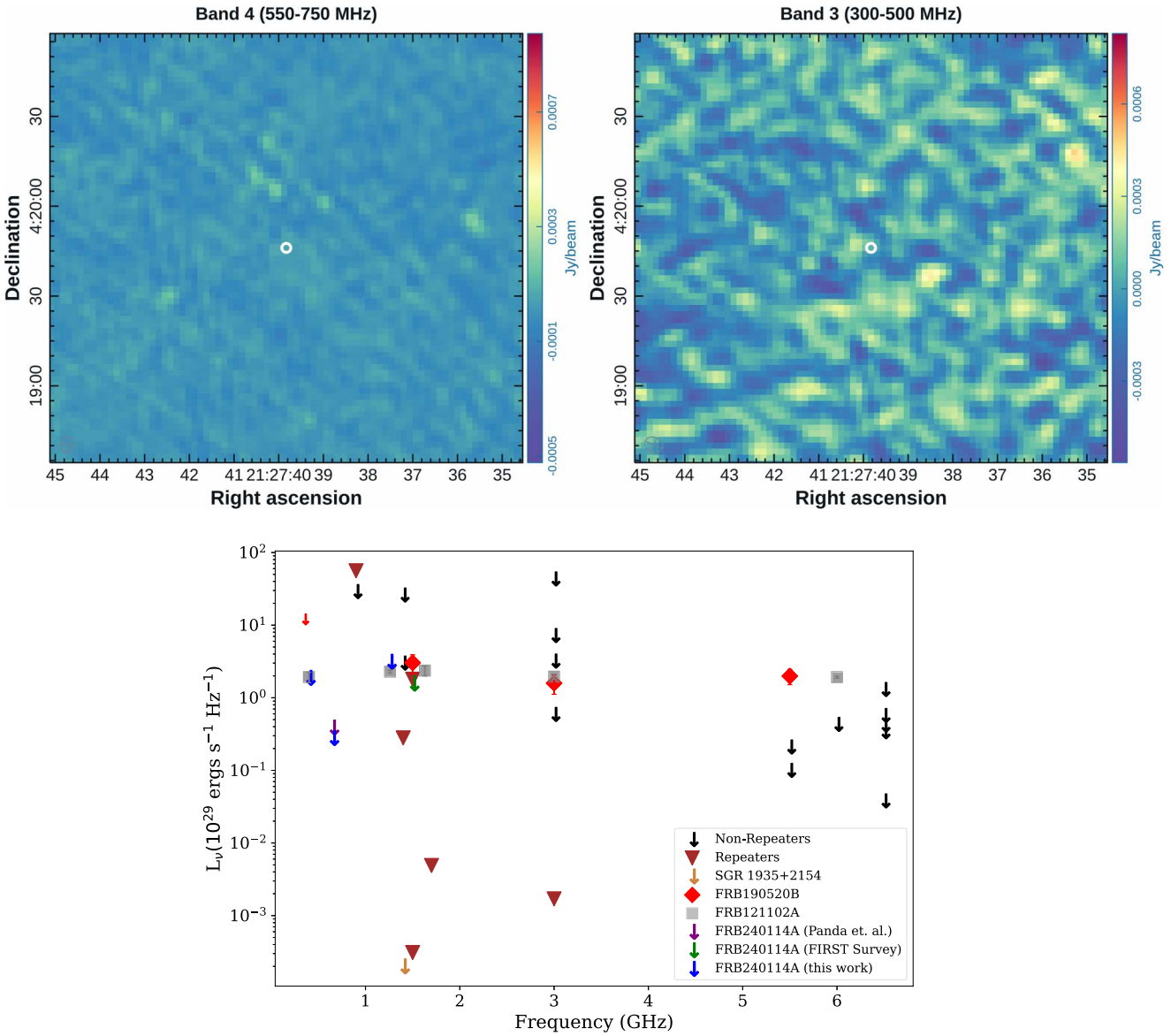

Figure 5. Top: images of the sky regions around the sky-position of FRB 20240114A, at 650 and 400 MHz. The MeerKAT localization of FRB 20240114A is marked with a circle at the center of the images. Bottom: comparison of upper limits and measurements of spectral luminosity of PRS, associated with repeating and nonrepeating FRBs, and SGR 1935+2154, along with our upper limits for FRB 20240114A at different frequencies. References: S. Chatterjee et al. (2017), L. Resmi et al. (2021), C. H. Niu et al. (2022), C. J. Law et al. (2022), X. Zhang et al. (2023). For the original references for upper limits on various repeaters, nonrepeating FRBs, and SGR 1935+2154, please see C. J. Law et al. (2022).

of May, despite regular observations earlier too. Hence, there is an indication of a potential chromaticity in the activity, where FRB 20240114A is becoming active at higher frequencies at the later epochs. Nondetection of any burst from our latest band 4 observation on 2024 May 29, also indicates a quenching of the burst activity at lower frequencies.

FRB 20180916B is the only FRB for which strong evidence of chromaticity in its activity has been seen (I. Pastor-Marazuela et al. 2021; Z. Pleunis et al. 2021b). Despite having only a moderate burst rate, the discovery of the chromaticity was aided by the knowledge of the underlying modulation period of FRB 20180916B. For FRB 20240114A, an underlying periodicity, if any, in its activity is yet to be detected. Moreover, the frequency chromaticity in FRB 20240114A appears to be opposite to that in FRB 20180916B, i.e., the burst activity at higher frequencies seems to be delayed in FRB 20240114A, while the opposite is true for FRB 20180916B.

We note that the currently available information on FRB 20240114A is not sufficient to establish or rule out the above potential chromaticity. For example, bursts in the 2−6 GHz frequency range have been detected by sensitive telescopes like Effelsberg and Nancay (D. M. Hewitt et al. 2024; P. Joshi et al. 2024; P. Limaye & L. Spitler 2024). However, the observations displayed for the 4−6 GHz range in Figure 1 are mostly by much smaller telescopes and different setups, e.g., with smaller bandwidths (O. S. Ould-Boukattine et al. 2024a). Any lack of subband searches might also have contributed to the sensitivity differences. Furthermore, the narrowband emission of the bursts combined with narrow observing bandwidths might also have been decisive. With more detailed information on various observing setups, it might be possible to conduct simulations to further probe whether there is indeed chromaticity in FRB 20240114A's activity; however, that is beyond the scope of this work. Nevertheless, a systematic, multifrequency

monitoring of the source is needed to better probe this potential chromaticity, as well as any underlying periodicity.

Furthermore, J. Zhang et al. (2024b) conducted observations on 2024 January 28 and 29 and February 1 and 4, detecting 38 bursts with a total on-source time of 2 hr. The inferred burst rate at approximately 1.1 GHz is $20\,\mathrm{hr}^{-1}$ above the fluence threshold of around 0.015 Jy ms. Assuming a mean power-law index of -1.5, the burst rate would be only $0.072\,\mathrm{hr}^{-1}$ at a fluence threshold of 0.64 Jy ms. However, we estimate the burst rate to be $2.6\,\mathrm{hr}^{-1}$ at 400 MHz from our first band 3 observation on 2024 February 8, indicating a sharp evolution of burst rate with observing frequency and/or time.

5.2. Spectrotemporal Properties

The width distribution (not shown but assessed separately) of the bursts we detected shows a median width of 4.3 ms at 400 MHz, which is larger than the median width of 1.4 ms reported at 650 MHz (U. Panda et al. 2024b). In the left panel of Figure 2, we see that the peak frequency of the majority of the bursts is above 400 MHz, potentially suggesting a preference for the emission frequencies to be above 400 MHz. However, there could also be detection biases, e.g., lower sensitivity in the lower half of band 3 due to the presence of RFI and scatter broadening. Most of the bursts in our sample show narrowband emission. Similar behavior has been observed at 600 MHz with CHIME and at L band with FAST (K. Shin & CHIME/FRB Collaboration 2024; J. Zhang et al. 2024b). Narrowband emission has also been observed in the giant pulses of the Crab pulsar and FRB 20190711A (P. Kumar et al. 2021; P. Thulasiram & H.-H. Lin 2021), with similar values of $\Delta\nu/\nu$ to those for FRB 20240114A. There is the possibility of bursts being narrow owing to emission being below our detection threshold at other frequencies and brightest at frequencies where we detect them, which effectively implies steep modulations in the burst spectra. J. M. Cordes et al. (2017) show that caustics can produce strong magnifications ($\leqslant 10^2$) in plasma and present as spectral peaks in the frequency range 0.1–1 GHz. Plasma lensing has been invoked to explain narrowband and high-energy bursts for repeating FRBs, e.g., FRB 121102A and FRB 201124A (X. Chen et al. 2024). B. D. Metzger et al. (2019) invoke synchrotron maser emission in ultrarelativistic magnetized shocks to produce the downward-drifting pattern. Under certain conditions, it predicts a simultaneous narrowband emission that is not intrinsic but most likely caused by the propagation effects, e.g., plasma lensing.

W.-Y. Wang et al. (2022) modeled the drift rates of various repeating FRBs as a function of frequency (in the rest frame of the host galaxy) with a power law. They suggest that the downward drift can be explained through curvature radiation in magnetars originating from different heights. Figure 4 shows that the drift rates we measured for FRB 20240114A also agree with the relationship modeled by W.-Y. Wang et al. (2022). In the lower frequency regime, FRB 180916B has been the only other FRB with such measurements. Our measurements for FRB 20240114A further populate this part of the phase space.

5.3. Energetics

Several bursts have now been reported from FRB 20240114A that have fluence in excess of 50 Jy ms (O. S. Ould-Boukattine et al. 2024a; O. S. Ould-Boukattine et al. 2024b; D. Pelliciari et al. 2024b; K. Shin & CHIME/FRB Collaboration 2024); however, all the bursts except one that we detected have fluences below 10 Jy ms (twice as high as CHIME/FRB's typical detection threshold). This might suggest that most of the time the source might be emitting relatively low energy bursts, also seen by J. Zhang et al. (2024b), and high-energy bursts might be following a different mean burst rate and power-law statistics. If this is really the case, it would remain to be seen whether the two populations of bursts are caused by different emission mechanisms or propagation effects (e.g., plasma lensing). Particularly for FRB 20201124A, F. Kirsten et al. (2024) argue that the higher-energy burst population cannot be explained by lensing effects and the increased brightness is intrinsic.

For FRB 20240114A, we obtain a power-law index of -1.24 ± 0.11 for the bursts we detected at 400 MHz. We note that, much like several other works following the same approach, our fluences are estimated from the band-averaged bursts, even for the bursts clearly having narrow bandwidths. Our measured power-law index of -1.24 ± 0.11 is consistent with those measured for several other repeaters, for which a wide range from a relatively flat index of -0.5 to as steep as -4.9 has been reported (F. Kirsten et al. 2024). This index also varies with time and the range of observed energies of the bursts (F. Kirsten et al. 2024). For FRB 20240114A, U. Panda et al. (2024b) fit a broken power law for bursts detected at 650 MHz with an index at the lower end of -0.7, which is flatter than what we measure at 400 MHz. While this could suggest a dynamic or frequency-dependent change in the energy distribution, it could also result from incompleteness in the search for lower-fluence bursts.

A similar power-law index has been measured for several other repeating FRBs, as well as the giant pulses from the Crab pulsar and the magnetar XTE 1810−197 (M. Serylak et al. 2009; Y. Maan et al. 2019). However, different measurements have resulted in different power-law indices for the same sources, indicating temporal evolution or a more complex distribution of the bursts.

5.4. Persistent Radio Source

PRSs have been associated with two repeating FRBs so far, FRB 20190520B and FRB 20121124A (S. Chatterjee et al. 2017; C. H. Niu et al. 2022). For both FRBs, there is temporal evolution of the associated PRS flux densities (G. Chen et al. 2023; L. Rhodes et al. 2023). Figure 5 shows the spectral luminosity of the PRS associated with the above two repeating FRBs at different frequencies, along with the upper limits for a few repeating and one-off FRBs, as well as our upper limits on the spectral luminosity of any PRS associated with FRB 20240114A at 400 and 650 MHz. Especially at 650 MHz, our upper limit is almost an order of magnitude below the spectral luminosity of the two known PRSs.

Two models have been invoked to explain the persistent radio emission—one involves a magnetized ion–electron nebula (B. Margalit & B. D. Metzger 2018), and the other involves a hypernebula, i.e., a hyperaccreting compact object (N. Sridhar & B. D. Metzger 2022). While our limits are quite stringent at lower frequencies, a spectral turnover around or above 1 GHz cannot be ruled out. In that case, it might still be possible to detect the PRS at higher frequencies. Furthermore, the turnover is expected to shift to lower radio frequencies with time (B. Margalit & B. D. Metzger 2018), and hence the PRS could also become detectable even at 650 MHz at a later epoch. In such a case, our current limits would be useful in

constraining the temporal evolution. Overall, regular sensitive observations at a few different frequencies would be useful to probe any associated PRS.

C. J. Law et al. (2022) studied any potential correlations between various burst properties, e.g., the repetition rate, and the associated PRS luminosity. An interesting idea is that the excess DM caused by the host galaxy, DM_{host}, might be causally connected to the PRS (C. J. Law et al. 2022). For FRB 20240114A, DM_{host} could be around 330 pc cm^{-3} (M. Bhardwaj et al. 2024), which is larger than the typical contribution from the interstellar medium in the host galaxies. When compared to the DM_{host} and repetition rate of FRBs with and without an associated PRS, FRB 20240114A's DM_{host} and repetition rate might favor the presence of a PRS. However, DM_{host} normalized by the stellar mass of the galaxy could be more informative (C. J. Law et al. 2022, e.g., their Figure 4).

6. Conclusions

We report detection of 60 bursts from FRB 20240114A at band 3 (300–500 MHz) and band 4 (550–750 MHz) of the uGMRT. We also confirm the lower-frequency counterpart of the burst storm that was reported at *L* band with a rate of 500 hr^{-1} using FAST on 2024 March 5, but with a burst rate of 31 hr^{-1} above a fluence threshold of 0.22 Jy ms for 2 ms wide bursts at 400 MHz. From a detailed analysis of our low-energy burst sample, as well as considering the reported detection of FRB 20240114A from other telescopes, we conclude the following:

1. The fluence distribution of the FRB 20240114A bursts at 400 MHz in the range 0.1−10 Jy ms is well fit with a single power-law index of -1.24 ± 0.11.
2. The bursts from FRB 20240114A exhibit narrowband (about 10% fractional bandwidth) behavior and a downward-drifting pattern similar to many other repeating FRBs. Our drift-rate estimates for FRB 20240114A are such measurements at the second lowest frequency for any FRB so far. The drift rates are consistent with the power-law fit for such estimates from various FRBs at their rest-frame frequencies and might indicate curvature radiation at different heights as the origin of the observed downward-drifting emission.
3. We place the most stringent upper limits at 400 and 650 MHz on the spectral luminosity of any underlying PRS associated with FRB 20240114A. The upper limit at 650 MHz is nearly an order of magnitude below the luminosity of the two known PRSs at this frequency. However, a spectral turnover at higher frequencies cannot be ruled out as the cause of the nondetection, and continued monitoring would be helpful.
4. Finally, FRB 20240114A shows frequency-dependent burst rate. By combining the information available from follow-ups at other telescopes and frequencies, we also show that the burst activity of FRB 20240114A is potentially frequency dependent. Our latest observation at band 4, also indicates a potential quenching of the activity at low frequencies.

Overall, the similarity of various properties of FRB 20240114A to other repeating FRBs suggests a common intrinsic nature of emission. Our results also warrant multi-frequency monitoring of FRB 20240114A to establish the potential frequency-dependent activity and probe a spectral turnover evolution of any associated PRS.

Acknowledgments

We would like to thank Ramananda Santra for useful discussions regarding interferometric data analysis. A.K. would like to thank Arvind Balasubramanian for useful discussions. We would like to thank the Centre Director and the observatory for the prompt time allocation and scheduling of our observations. Y.M. acknowledges support from the Department of Science and Technology via the Science and Engineering Research Board Startup Research grant (SRG/2023/002657). We acknowledge the Department of Atomic Energy for funding support, under project 12−R&D−TFR−5.02−0700. GMRT is run by the National Centre for Radio Astrophysics of the Tata Institute of Fundamental Research.

Facilities: GMRT.

Software: astropy (Astropy Collaboration et al. 2013), matplotlib (J. D. Hunter 2007), scipy (P. Virtanen et al. 2020), your (K. Aggarwal et al. 2020), RFIClean (Y. Maan et al. 2021), PRESTO (S. Ransom 2011).

ORCID iDs

Ajay Kumar https://orcid.org/0009-0002-0330-9188
Yogesh Maan https://orcid.org/0000-0002-0862-6062
Yash Bhusare https://orcid.org/0000-0002-5342-163X

References

Aggarwal, K., Agarwal, D., Kania, J., et al. 2020, JOSS, 5, 2750
Astropy Collaboration, Robitaille, T. P., Tollerud, E. J., et al. 2013, A&A, 558, A33
Bannister, K. W., Deller, A. T., Phillips, C., et al. 2019, Sci, 365, 565
Bhandari, S., Sadler, E. M., Prochaska, J. X., et al. 2020, ApJL, 895, L37
Bhardwaj, M., Kirichenko, A., & Gil de Paz, A. 2024, ATel, 16613, 1
Bochenek, C. D., Ravi, V., Belov, K. V., et al. 2020, Natur, 587, 59
Cash, W. 1979, ApJ, 228, 939
Chamma, M. A., Rajabi, F., Kumar, A., & Houde, M. 2023, MNRAS, 522, 3036
Chatterjee, S., Law, C. J., Wharton, R. S., et al. 2017, Natur, 541, 58
Chen, G., Ravi, V., & Hallinan, G. W. 2023, ApJ, 958, 185
Chen, X., Hu, B., Wang, P., et al. 2024, MNRAS, 531, 4155
CHIME/FRB Collaboration, Amiri, M., Andersen, B. C., et al. 2020a, Natur, 582, 351
CHIME/FRB Collaboration, Andersen, B. C., Bandura, K., et al. 2019, ApJL, 885, L24
CHIME/FRB Collaboration, Andersen, B. C., Bandura, K. M., et al. 2020b, Natur, 587, 54
Cordes, J. M., Wasserman, I., Hessels, J. W. T., et al. 2017, ApJ, 842, 35
Feng, Y., Li, D., Zhang, Y.-K., et al. 2023, ApJ, 974, 296
Fonseca, E., Andersen, B. C., Bhardwaj, M., et al. 2020, ApJL, 891, L6
Gopinath, A., Bassa, C. G., Pleunis, Z., et al. 2024, MNRAS, 527, 9872
Gupta, Y., Ajithkumar, B., Kale, H. S., et al. 2017, CSci, 113, 707
Heintz, K. E., Prochaska, J. X., Simha, S., et al. 2020, ApJ, 903, 152
Hessels, J. W. T., Spitler, L. G., Seymour, A. D., et al. 2019, ApJL, 876, L23
Hewitt, D. M., Huang, J., Hessels, J. W. T., et al. 2024, ATel, 16597, 1
Hunter, J. D. 2007, CSE, 9, 90
Joshi, P., Medina, A., Earwicker, J. T., et al. 2024, ATel, 16599, 1
Kale, R., & Ishwara-Chandra, C. H. 2021, ExA, 51, 95
Kirsten, F., Ould-Boukattine, O., Herrmann, W., et al. 2024, NatAs, 8, 337
Kumar, A., Maan, Y., & Bhusare, Y. 2024, ATel, 16452, 1
Kumar, P., Luo, R., Price, D. C., et al. 2023, MNRAS, 526, 3652
Kumar, P., Shannon, R. M., Flynn, C., et al. 2021, MNRAS, 500, 2525
Lanman, A. E., Andersen, B. C., Chawla, P., et al. 2022, ApJ, 927, 59
Law, C. J., Connor, L., & Aggarwal, K. 2022, ApJ, 927, 55
Limaye, P., & Spitler, L. 2024, ATel, 16620, 1
Maan, Y., Joshi, B. C., Surnis, M. P., Bagchi, M., & Manoharan, P. K. 2019, ApJL, 882, L9
Maan, Y., van Leeuwen, J., & Vohl, D. 2021, A&A, 650, A80

Marcote, B., Nimmo, K., Hessels, J. W. T., et al. 2020, Natur, 577, 190
Margalit, B., & Metzger, B. D. 2018, ApJL, 868, L4
Marthi, V. R., Gautam, T., Li, D. Z., et al. 2020, MNRAS, 499, L16
Metzger, B. D., Margalit, B., & Sironi, L. 2019, MNRAS, 485, 4091
Niu, C. H., Aggarwal, K., Li, D., et al. 2022, Natur, 606, 873
Ould-Boukattine, O. S., Dijkema, T. J., Gawronski, M., et al. 2024a, ATel, 16565, 1
Ould-Boukattine, O. S., Hessels, J. W. T., Kirsten, F., et al. 2024b, ATel, 16432, 1
Panda, U., Bhattacharyya, S., Dudeja, C., Kudale, S., & Roy, J. 2024a, ATel, 16494, 1
Panda, U., Roy, J., Bhattacharyya, S., Dudeja, C., & Kudale, S. 2024b, arXiv:2405.09749
Pastor-Marazuela, I., Connor, L., van Leeuwen, J., et al. 2021, Natur, 596, 505
Pelliciari, D., Geminardi, A., Bernardi, G., et al. 2024a, ATel, 16434, 1
Pelliciari, D., Geminardi, A., Bernardi, G., et al. 2024b, ATel, 16547, 1
Pleunis, Z., Good, D. C., Kaspi, V. M., et al. 2021a, ApJ, 923, 1
Pleunis, Z., Michilli, D., Bassa, C. G., et al. 2021b, ApJL, 911, L3
Rajwade, K. M., Mickaliger, M. B., Stappers, B. W., et al. 2020, MNRAS, 495, 3551
Ransom, S., 2011 PRESTO: PulsaR Exploration and Search TOolkit, Astrophysics Source Code Library, ascl:1107.017
Resmi, L., Vink, J., & Ishwara-Chandra, C. H. 2021, A&A, 655, A102
Rhodes, L., Caleb, M., Stappers, B. W., et al. 2023, MNRAS, 525, 3626
Serylak, M., Stappers, B. W., Weltevrede, P., et al. 2009, MNRAS, 394, 295
Seymour, A., Michilli, D., & Pleunis, Z., 2019 DM_phase: Algorithm for correcting dispersion of radio signals, Astrophysics Source Code Library, ascl:1910.004
Shin, K. & CHIME/FRB Collaboration 2024, ATel, 16420, 1
Snelders, M. P., Bhandari, S., Kirsten, F., et al. 2024, ATel, 16542, 1
Spitler, L. G., Cordes, J. M., Hessels, J. W. T., et al. 2014, ApJ, 790, 101
Sridhar, N., & Metzger, B. D. 2022, ApJ, 937, 5
Thulasiram, P., & Lin, H.-H. 2021, MNRAS, 508, 1947
Tian, J., Pastor-Marazuela, I., Stappers, B., et al. 2024, ATel, 16446, 1
Uttarkar, P. A., Kumar, P., Lower, M. E., & Shannon, R. M. 2024, ATel, 16430, 1
Virtanen, P., Gommers, R., Oliphant, T. E., et al. 2020, NatMe, 17, 261
Wang, W.-Y., Yang, Y.-P., Niu, C.-H., Xu, R., & Zhang, B. 2022, ApJ, 927, 105
Zhang, J., Wu, Q., Cao, S., et al. 2024a, ATel, 16505, 1
Zhang, J., Zhu, Y., Cao, S., et al. 2024b, ATel, 16433, 1
Zhang, X., & Yu, W. 2024, ATel, 16695, 1
Zhang, X., Yu, W., Law, C., et al. 2023, ApJ, 959, 89
Zhou, D. J., Han, J. L., Zhang, B., et al. 2022, RAA, 22, 124001